A TES Finline Detector for Bolometric Interferometry

Louisa Dunlop*, David Goldie*, Stafford Withington*, Dorota Glowacka* and Ghassan Yassin†
*Detector Physics Group, Cavendish Laboratory,
University of Cambridge,
Madingley Road, CB3 0HE, UK
† Department of Physics, University of Oxford, Denys Wilkinson Building,
Keble Road, Oxford, OX1 3RH, UK

***Abstract*— We present work on a highly unusual single-chip antenna-coupled bolometric interferometer for high performance applications at 150 GHz. The design of the detector is suitable for many areas of astronomical research ranging from Sunyaev–Zeldovich (SZ) mapping through to B-mode polarisation measurements of the CMB. The design employs corrugated feedhorns for coupling the astronomical signal to the detectors. This arrangement provides a well–collimated beam with low side lobes and low cross polarization. Two back-to-back finline tapers couple the incoming waveguide modes to a single chip, where a miniature microstrip hybrid coupler and pair of Mo/Cu microstrip coupled TES detectors are located. The scheme overcomes mechanical restrictions associated with the geometry of the waveguide. Numerous extensions to the basic technique are now possible.**

I. Introduction

Low temperature TES detectors are widely used for ground, balloon and satellite based millimetre and sub millimeter wave astronomy. The current state of the art technology is to develop microstrip coupled TES detectors [1]. Here at Cambridge we offer the next stage polarisation detector that employs these detectors in an interferometric arrangement. This will be be useful for high performance applications in many different areas of research including: SZ mapping, where for the thermal SZ one sees a significant decrement in Intensity, interferometric mapping of dust at wavelengths between 3mm and 300μm and CMB B-mode polarisation measurements.

With our design we demonstrate how it is possible to construct a single chip interferometer based on known SQUID and TES technology. The detector chip and block designs are based on our finline mixer work that has been reported in several publications [2]. Our scheme will produce cos and sin fringes directly and with a slight modification could be used for single chip polarimetry. This is an extremely versatile design that will benefit many areas of astronomy in the future.

II. The single chip Interferometer

In the first phase of the project, the two element interferometer comprises of two identical broadband corrugated horn antennas machined into an aluminium spilt-block. The chip sits in a recess in the chip block. A schematic view of the chip is shown in Fig.1. The signals from the two horns are fed to a back-to-back finline taper that transforms the waveguides into niobium superconducting microstrip. The two inputs from the opposite microstrips are then combined by a 4-port 180° hybrid that provides the sum ($E_1 + E_2$) and the difference ($E_1 - E_2$) at either output [3]. Each output is transferred via microstrip to a matched resistor that lies on the TES membrane. The RF power is converted into heat, which causes a sharp increase in the Voltage Biased TES resistance. This reduces the bias current which is read by a Superconducting Quantum Interference Device (SQUID). Transferring the signal from waveguide to microstrip allows the circuitry to become independent of the waveguide geometry, therefore the substrates size and shape between the tapers are now restricted only by the TES and miniature microstrip hybrid coupler.

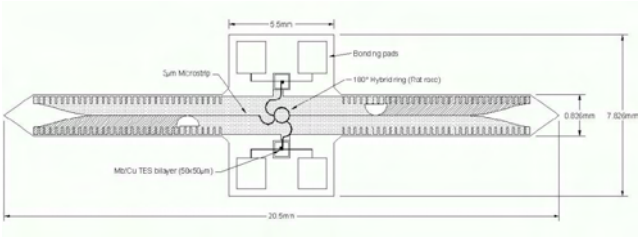

Fig. 1. The Design for the chip as created on AutoCAD. This shows the layout of all the components that will be processed using lithography techniques.

A. Feed horns

The corrugated feed horn selects the HE_{11} mode which provide a symmetric main beam with a low side lobe response. The Gaussian beam mode diffraction method is suitable for sub mm beam characterisation. This method of analysis provides a reasonable understanding of the profile of the beam throughout the system and allows the element sizes and beam pattern to be calculated using simple formulae [4]. Corrugated feed horns have been designed using the software CORRUG. They possess a 12 degree pitch angle and have a return loss of -22.9 dB at 150GHz. There is excellent matching between the E and H Plane in this design shown in Fig.2. A disadvantage of the Gaussian Beam assumption is that the beam is not of infinite extent, therefore the effect of the aperture on the beam must be considered and this is discussed in [5].

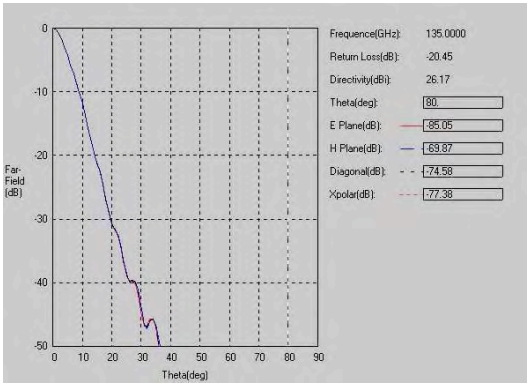

Fig. 2. A diagram to show the beam pattern of our corrugated horn feed.

B. Finline Taper

The antipodal finline taper allows the merger of two desirable techniques for our detector. Transforming the waveguide into microstrip not only allows the implementation of high performance horns but also enables the electromagnetic design from finline to detector to be fabricated using planar circuit technology. This creates a highly reproducible technique that will be required to allow compact packaging of detectors with increasing and variable baselines which will, as a consequence, increase the sensitivity of the device. The finline taper is constructed from two superconducting niobium films that are deposited on one side of a silicon substrate and are isolated by a $400\,\mathrm{nm}$ SiO_2 layer. Before the fins overlap the SiO_2 is significantly thinner than the Si wafer, therefore the transmission line behaves as a unilateral finline on a Silicon substrate. At this stage the impedance is several hundred ohms [2] assuming a dielectric constant of Si and SiO_2 are 11.7 and 3.8 respectively. As the fins overlap the structure behaves like a parallel plate waveguide with an effective width equal to the overlap region. As soon as the overlap is significant, fringing can be ignored and the fins can be tapered to form microstrip. At this stage it is the SiO_2 that determines the electrical properties of the microstrip. For a microstrip width $w \approx 3\mu$m and a thickness $t \approx 400$nm we obtain an impedance value $Z_0 \approx 20\Omega$. A circular arc transforms the antipodal finline to microstrip by extending the base fin to form the ground plane at the same time as tapering the top fin inwards until a width of 3μm is achieved. The finline design, a combination of the unilateral, antipodal and circular arc sections, is displayed in Fig.3. It should be noted that even with the use of the optimum

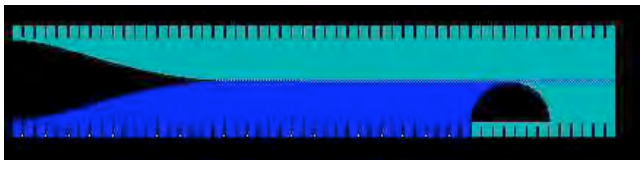

Fig. 3. The completed finline constructed with the use of 4 programs in total, 3 existing Fortran 77 programs and one written in the C programming language.

taper method, where the coupling coefficient is minimised between the incident and reflected waves in the z-direction, there may be reflections from the front surface of the chip. This may be minimised with the use of a quarter wave transformer. In our design a 0.5 *mm* high triangular section was designed and was successfully fabricated.

C. The 180° Hybrid Ring and the matched resistor

The Rat Race hybrid ring was chosen over the Wilkinson combiner for its ease of processing (i.e. no resistors) and because it is ideal for our geometry that employs two TES detectors. The hybrid produces the required output with a low return loss, although over a relatively narrow bandwidth. It consists of a 4-port network made of microstrip that has a 180° phase shift between the two output ports [3].

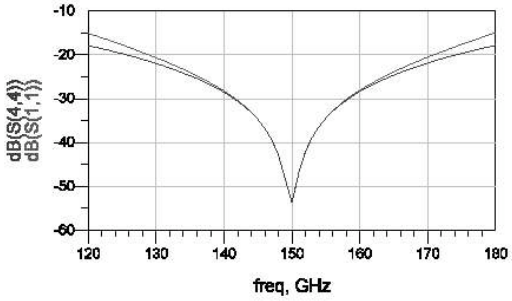

Fig. 4. The Reflection parameter (S11) of the rat race as simulated using ADS.

The ring has impedance $\sqrt{Z_0}$ where Z_0 has a value of 20 Ω. This requires a microstrip of width, $W \approx 2\mu$m, in the ring. When ports 2 and 3 are used as the inputs of the rat race then the outputs provide a combined signal. The sums and differences of the inputs are taken at ports 1 and 4 respectively. The rat race was modelled using Automated Design System (ADS) and was found to provide a bandwidth of around 30GHz, shown in Fig.4. The bandwidth could be extended further if required with the addition of extra rings. The two outputs from the combiner are taken to opposite sides of the chip by two superconducting microstrips that reach the TES membranes where each is terminated by a matched resistor close to a TES. Optimising the space available on the TES island, ensuring minimal reflection and the feasibility of processing were important considerations when designing the resistor termination. The resistor was modelled using Sonnet em software. For z=24.5Ω and a 3 μm wide Gold/Copper resistor with a resistivity of $1.02\pm0.18\times10^{-7}$ and a thickness of 42nm, a length of 30.5mm is required.. The simulation confirmed that good termination is possible providing a return loss of around -20dB at 150GHz.

D. Cryostat

A Janis Liquid Helium Dewar hosts a 3 stage Sub-kelvin Helium 3 cooler developed by Chase Research Cryogenics Ltd. The Dewar has a nitrogen and helium reservoir both

of which are surrounded by a vacuum in order to isolate the reservoirs from room temperature. The interior of the Dewar is constructed from Stainless steel which has a low thermal conductivity and is extremely robust, therefore it can withstand many cycles between room temperature and helium temperature. The Chase fridge contains a sealed ^{3}He system. The ^{4}He is transferred to the ultrahead and cools it to 4K then the charcoal pump is cooled to below 20K and absorbs the ^{4}He. This decreases the pressure and cools the fridge to its condensation point.It is important that all the ^{4}He is depleted otherwise the ^{4}He will form a super-fluid and will have a negative effect on the performance of the system. Next the ^{3}He is released into the inner chamber of the ultrahead. The charcoal is used in the same way until the desired temperature is reached at which time the charcoal temperature is once again increased. The hold time before all of the liquid ^{3}He has boiled off is 7 hours. Thermal straps are required as a thermal link to the chase fridge which will reduce and sustain the temperature of the chip block at around 250mK. The metal surfaces of the table and the chip block are gold plated to ensure good thermal contact and low emissivity. Low Pass filters are placed on the radiation shields and on the table to prevent the transmission of the Blackbody radiation at high T. This is achieved by controlling the wavelengths of the radiation that pass. The window is constructed from a 1.3mm thickness of high density polyethene that has a 100% transmission at 150GHz [5]. The magnetic shielding is an important feature

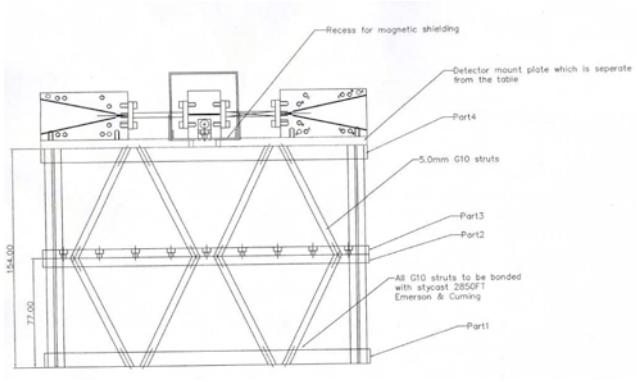

Fig. 5. A CAD drawing of the cryostat interior.

of the design because it prevents external magnetic fields from penetrating the TES bilayer. The attenuation of a magnetic field can be accomplished by inserting a screen made from a magnetic material with a high permeability ($\mu \gg 1$) between the source and the sensitive component. The inner field is reduced because the external magnetic field tends to remain in the magnetic layer of the shield because it offers a low-reluctance path. The shielding factor of the magnetic shield is defined as,

$$S = \frac{H_a}{H_i}, \tag{1}$$

where H_a is the external field strength and H_i is the residual internal field strength. It is typical to calculate a shielding factor for a sphere or a cylinder however these shapes are not always the most practical. It was decided that a cuboid structure was best suited to our design, however it was noted that magnetic flux lines prefer not to turn by 90 degrees and a cylindrical or spherical shape would have been more efficient at restricting the magnetic field. The shielding effect of a cube with edge length a is,

$$S_c = \frac{4}{5}.\frac{\mu_r.d}{a} + 1, \tag{2}$$

This is an average shielding factor, with the value of S less in the centre compared to at the edges; therefore the smaller the value a, the better. The geometry of the shield is kept simple in order to ensure magnetic continuity i.e the flux can continue along the low reluctance path. Our design incorporates a base tray that will hold the cuboid shield. This then allows the structure to be secured on the bottom edge. The design aims to minimise the number of openings and only contains unavoidable openings where necessary, for example the waveguide and thermal straps must pass through to the rest of the system. The cuboid structure can be slid over the waveguide by cutting two slits in opposite sides of the box. An external cover will be fixed to cover any unnecessary gaps. For our shield we have chosen to use Cryoperm 10. This is an ideal material for our application because its permeability increases with decreasing temperature. The influence of openings has been studied closely for common magnetic shield shapes like the cylinder. We have calculated an approximate value for the cuboid structure that follows the previous work by Vacuumchmetlz. The exponential relationship between the field and the distance travelled past the gap is also an important consideration. It is generally accepted that a 3/1 ratio of gap diameter and length of shield is the best for this application. Our Shielding factor has been calculated to be 1217.39 ignoring holes, but a more realistic worse case scenario is of the order 577. This gives an internal field of 0.097 $\frac{A}{m}$. inserting multiple magnetic shields would increase the shielding factor and as a consequence decrease the internal magnetic field. The shield is mounted on a copper strip of width 48mm and depth 6mm which is itself mounted on a custom built table. The copper strip will also be cooled to the required temperature by two straps that are linked to the chase fridge.

III. Detector Readout

A. Introduction

The TES is a $50 \times 50\mu m^2$ superconducting molybdenum/copper film of thickness 40nm and 30 nm respectively, deposited on a 1μm membrane of silicon nitride. A constant voltage source is used to bias the device in the middle of the transition between the normal and the superconducting states. Incident RF power creates a small increase in the device temperature which causes a large change in resistance allowing the detection of very weak signals.

$$\alpha = \frac{d(logR)}{d(logT)}. \tag{3}$$

Figure 6 shows how we model the TES as a variable resistor

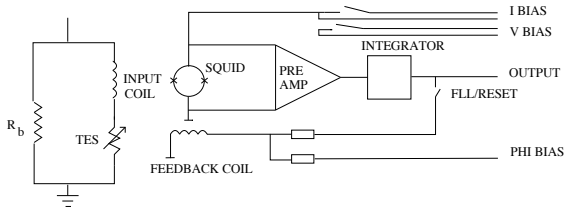

Fig. 6. A diagram to show the set up of a TES with ETF.

in a voltage bias circuit. The constant bias voltage leads to an Electro-Thermal Feedback signal (ETF) that keeps the device biased in the middle of the transition. This occurs because increasing the resistance of the TES decreases the bias current and therefore the bias power, keeping the detector at a constant temperature. The signal is then detected as a reduction in the bias current which is read by a SQUID. We are in the process

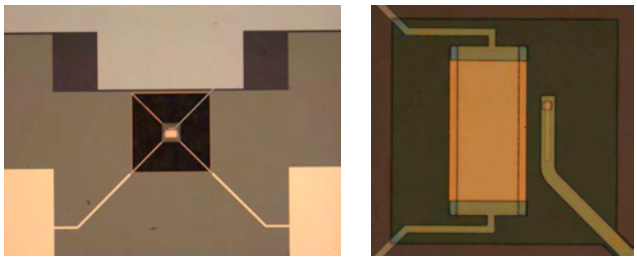

Fig. 7. (Left) The TES membrane is the central region on the plot. The length of the thermal links are 350 μm each. We have experienced signifi cant success with the processing of the membrane using our wet etching tecnique which utilises 20% KOH at 80°C. (Right) The TES detectors have been successfully fabricated in our laboratory. The Au/Cu termination resistor, the niobium bias lines and the copper banks can be seen clearly.

of fully characterising the noise associated with our system. We expect our results to match noise theory [6]:

$$\begin{aligned} NEP^2 &= NEP_{ph}^2 + NEP_{jn}^2 + NEP_{sq}^2 + {NEP_{\rm excess}}^2; \\ NEP_{ph}^2 &= \gamma 4kT_c^2 G, \\ NEP_{jn}^2 &= \frac{4kT}{\mid Si \mid^2 R}\left(\frac{\tau}{\tau_0}\right)^2\left(\frac{1+\omega^2\tau_0^2}{1+\omega^2\tau^2}\right), \\ NEP_{sq}^2 &= \frac{i_{squid}^2}{\mid Si \mid^2}, \end{aligned} \tag{4}$$

where γ is a factor that takes into account the temperature gradient along the thermal link, G is the thermal conductance and Si is the responsivity of the TES. The terms in the above equation represent the phonon noise, a consequence of thermal fluctuations between the the TES and the heat sink, Johnson noise, SQUID noise and excess noise associated with the system. The SQUID noise is a measure of the noise associated with the readout including the SQUID and the pre-amplifier. Assuming that the detector is phonon noise limited reduces equation (4) to,

$$NEP^2 = \gamma 4k_b T_c^2 G(T_c). \tag{5}$$

Since γ remains constant, The $NEP_{\rm phonon}$ depends strongly on G and T_c . This implies that G must have an optimum value to obtain the best NEP of the device. If the value for G is too low the TES heats up increasing the undesired phonon noise. The temperature dependence of the conductance is given as,

$$G = nKT^{(n-1)}, \tag{6}$$

and the power flow equation is given as

$$P = K(T_c^n - T_b^n). \tag{7}$$

The minimum NEP can be obtained when $T_c \approx 2T_b$ where T_b is the temperature of the heat bath. An expression for the optimum $G(T_c)$ is given as,

$$G_{opt}(T_c) = \frac{n}{1-\left(\frac{T_b}{T_c}\right)^n}\frac{\beta P_{opt}}{T_c}, \tag{8}$$

where,

$$\beta - 1 = \frac{\frac{V_b^2}{R}}{P_{opt}}, \tag{9}$$

which depends on the ratio of Joule heating to background power heating. This value is predicted to be $250\frac{pW}{K}$ where P_{opt} =10pW, $T_c = 440mK$, n≈3 and β =3. The SQUID is a flux to voltage converter and will be used to read out the minute changes in current from the TES. A SQUID consists of two resistively shunted josephson junctions on a loop of superconducting inductance, L. In a closed loop made of superconducting material, the flux is quantised. The periodicity of the quantization is known as the flux quantum and is given as $2.07\times10^{-15}Wb$. When there is zero flux present a constant bias current, I_b is applied to the SQUID that divides equally between the junctions. When a current passes through the input coil, see Fig.6, magnetic flux is induced through itself and the SQUID, Φ_0. This generates a current in the loop of the SQUID that adds to the bias current in one junction and subtracts it in the other. The resulting flux in the SQUID is converted into a signal voltage, $V_s = \Phi\frac{dV}{d\Phi}$. This voltage is amplified and then passed through a feedback resistor and the resulting current flows though a feedback coil and causes a feedback flux, $-\Phi_F = -MI_F$ in the SQUID, where M is the mutual inductance between the feedback coil and the SQUID. The feedback flux cancels the external flux allowing the SQUID to act as a null detector [7].

IV. Preliminary noise and Dark NEP measurements

Initial measurements of our TES detectors have been carried out in an Oxford Instrument Heliox that has a base temperature of 250mK and multiple superconducting and Cryoperm shielding to reduce the incident magnetic field. We are using SuperSQUID designed by Polushkin et al [7] and fabricated by ourselves in the Detector Physics groups clean room facility at the Cavendish Laboratory. The input coil is coupled to the SuperSQUID with a mutual inductance of 25pH and the feedback coil has a mutual inductance of 0.75pH. The large V$-\phi$ and low noise pre–amp give a current noise $< 1\frac{pA}{\sqrt{Hz}}$

and a bandwidth in excess of 1MHz in the Flux Locked Loop mode. The circuit in Fig.6 was constructed and a

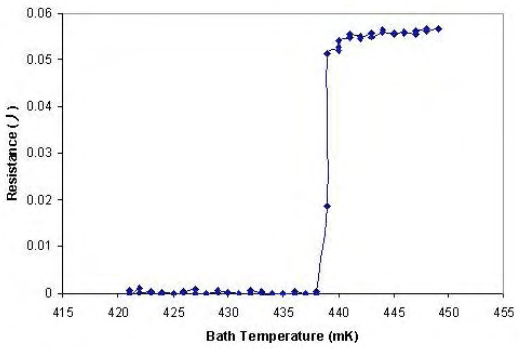

Fig. 8. A plot of the Resistance against Temperature for our 176_2 TES detector.

set of IV curves of varying input bias voltages were taken to provide the relationship between power and temperature. Plotting power against the bath temperature, Fig.9, allowed us to determine the key parameters associated with the power flow (7). From the results K and n were calculated to be 490 $\frac{pW}{K^n}$ and 2.95 respectively. A transition temperature of 440mK is displayed on our resistance against temperature plot in Fig.8. The thermal conductance for our Mo/Cu TES detectors, that are positioned on a 1μm of silicon nitride, is given by (6) [8] and using the variables above is calculated to be 291pW/K for a transition temperature of 440 mK. These measurements have been obtained for a membrane with thermal bridges of width 14μm and length 350μm. Work on the time constant for this device will be presented shortly. Noise characteristics of the

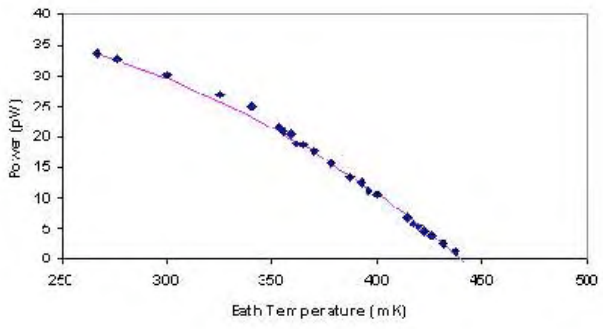

Fig. 9. A plot of the power flow against bath temperature.The points are the measured data and the line is the predicted values using equation (eq:power).

device, Fig.10 allow us to independently determine the NEP of the TES to be $4.5 \times 10^{-17} \frac{W}{\sqrt{Hz}}$ which agrees well with the value calculated substituting our value of G into (5). We are currently developing theoretical models that will complement a variety of our results.

V. Discussion

We have presented the design of a two element bolometric Interferometer that employs antenna coupled TES detectors

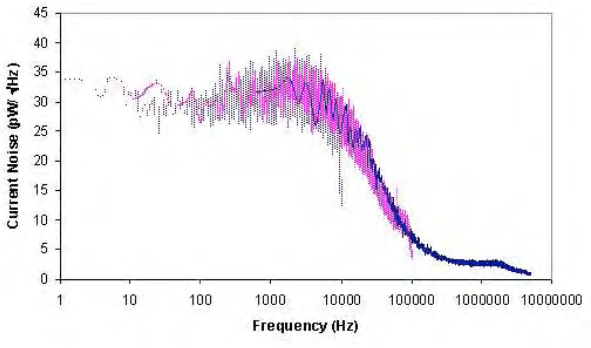

Fig. 10. Dark Current noise measurements of our 176_2 Mo/Cu TES detector for varying filter cutoffs of 10k, 100k and fout which had zero artificial frequency cutoff. Data is taken for a bias voltage of 1.2 μV at 251mK.

and corrugated horn feeds for good beam circularity and low cross polarisation. Development of the device and the test system is well advanced and we have a reproducible technique for the processing of sensitive TES detectors.

Future work will include the development of microstrip filters that will be inserted between the antenna and the TES. This will replace optical filters that are mounted on the cryostat.

References

[1] M. Yun *et al.*, "Fabrication of antenna-coupled transition edge polarization-sensitive bolometer arrays," *Nuclear Instruments and Methods in Physics Research A*, vol. 520, pp. 487–489, 2004.

[2] G.Yassin *et al.*, "A 350- ghz antipodal finline mixer," in *Proc. IEEE Transactions on Microwave Theory and Techniques*, vol. 48, April 2000.

[3] D. M. Pozar, *Microwave Engineering*, 2nd ed. New York: John Wiley & Sons inc, 1998.

[4] T. Edwards and M. Steer, *Foundations of Interconnect and Microstrip Design*, 3rd ed. John Wiley & Sons Ltd, 2000.

[5] P. F. Goldsmith, *Quasioptical Systems*. IEEE Press/ Chapman & Hall Publishers Series on Microwave Technology and RF, 1998.

[6] S.Lee *et al.*, "Voltage-biased superconducting transition-edge bolometer with strong electrothermal feedback operated at 370mk," *Applied Optics*, vol. 37(16), June 1998.

[7] V. Polushkin *et al.*, "A tightly coupled dc squid with an intermediary transformer," *Physica C*, vol. 72, 1998.

[8] M. Leivo and J. Pekola, "Thermal characteristics of silicon nitride membranes at sub-kelvin temperatures," *Applied Physics Letters*, vol. 367, 2002.